

Estimating relationships between snow water equivalent, snow covered area, and topography to extend the Airborne Snow Observatory dataset

Dominik Schneider^{1,2}, Noah P. Molotch^{1,2,3,*}, Jeffrey S. Deems⁴

Correspondence to: noah.molotch@colorado.edu

¹Dept. of Geography, Guggenheim 110, 260 UCB, Boulder Colorado 80309, USA

²Institute of Arctic and Alpine Research, University of Colorado Campus Box 450, Boulder, CO 80309, USA

³Jet Propulsion Laboratory, California Institute of Technology, 4800 Oak Grove Drive, Pasadena, CA 91109, USA

⁴National Snow and Ice Data Center, CIRES, 449 UCB, University of Colorado, Boulder, CO, 80309, USA

Abstract

A new spatio-temporal dataset from the ongoing Airborne Snow Observatory (ASO) provides an unprecedented look at the spatial and temporal patterns of snow water equivalent (SWE) over multiple years in the Tuolumne Basin, California, USA. We found that fractional snow covered area (fSCA) significantly improves our ability to model the distribution of SWE based on relationships between SWE, fSCA, and topography. Further, the broad availability of satellite images of fSCA facilitates the transfer of these relationship to different years with minimal degradation in performance compared with models fit on the same day, by considering variations in SWE depth as expressed by differences in fSCA between years. The crux of this proposition is in selecting the model to transfer. We offer a method with which to select a model from another year based on the similarity in SWE distribution at existing snow pillows in the area; the selected predictions exhibit a mild decrease in r^2 (0.02) and moderate increases in %MAE (15%) and %Bias (10%) from the best transferred predictions ($r^2=0.83$, %MAE=33%, %Bias=1%). The results motivate further refinement in the technique used to select the *best model* because if these dates can be identified then SWE can be modeled at accuracy levels equivalent to models generated from ASO data collected on the day of interest. Lastly, we found that models from ASO observations of anomalously low snowpacks in 2015 still transferred to other years, although the same cannot be said for the reverse. This research provides a first attempt at extending the value of ASO beyond the observations and we expect ASO will continue to provide insights for improving water resource management for years to come.

1 Introduction

The spatial distribution of snow water equivalent (SWE) largely controls the timing and magnitude of streamflow (Stewart et al., 2004) and is important for ecology (Giersch et al., 2016; Litaor et al., 2008) in snow-dominated catchments around the world. In these catchments, accurate assessments of snowpack water storage are critical for ensuring robust estimates of seasonal water supply. Nevertheless, SWE is poorly measured operationally with only sparse point measurements on the order of one measurement location per thousand square kilometers of snow covered terrain in the western United States (Meromy et al., 2012; Rice and Bales, 2010). Additional manual measurements in the form of snow courses add little information about the spatial variability and typically occur on the order of only three times a season (López-Moreno et al., 2013).

Satellite remote sensing provides spatially explicit information about the snowpack but current satellites are unable to measure SWE directly at the scales relevant for water resources management in mountainous terrain (e.g. the western United States) (Dozier, 2011). The need for improved information regarding the quantity and distribution of SWE has led to the development of new measuring techniques including the application of ground penetrating radar (GPR) (Marshall and Koh, 2008), Global Positioning Systems (GPS) (Gutmann et al., 2012; Koch et al., 2014), Light Detection and Ranging (lidar) (Deems et al., 2013; Prokop, 2008; Schirmer et al., 2011), and photogrammetry (Bühler et al., 2015; Nolan et al., 2015). Although these techniques are typically limited to snow depth, snow depth can be converted to SWE using modeled snow density or in situ snow pit observations (Elder et al., 1991; Jonas et al., 2009; Painter et al., 2016; Sturm et al., 2010).

Airborne systems have significantly improved the ability to measure SWE distribution at high spatial resolution and at extents relevant to water resource management (i.e. $> 100 \text{ km}^2$). However, most previous studies of snow distribution using airborne data have been limited to snap-shots in time, limiting the ability to empirically transfer observations to time periods outside of those directly sampled. Since 2013, the National Aeronautics and Space Administration (NASA), Jet Propulsion Laboratory, Airborne Snow Observatory (ASO) has acquired weekly observations of snow properties from approximately the time of annual peak SWE to the end of the snowmelt season in the Tuolumne Basin, California totaling 28 flights from 2013-2016 (Painter et al., 2016). ASO measures snow depth by differencing the lidar-derived elevations from snow-on and snow-off flights and infers albedo and snow extent based on spectroradiometric measurements. Density is computed using the iSNOBAL energy-balance model (Marks et al., 1999) based on inferred albedo, local meteorological measurements, and constrained by in situ snow pillow observations and manual snow course observations (Painter et al., 2016). Estimated snowpack density is multiplied by the lidar-derived snow depth to estimate SWE. These weekly observations of SWE distribution over multiple years represent a new opportunity for understanding the spatial and temporal dynamics of snow distribution. Moreover, the intensive repeat sampling of ASO may provide an opportunity to extend observed SWE patterns beyond the time periods directly observed by ASO – a goal of the work presented here. In this context, the ability to extend expensive ASO data in time could dramatically expand the applicability of ASO data to future time periods without incurring the costs associated with future airborne acquisitions.

A potential application of ASO measurements relates to the possibility of developing statistical relationships between ASO data and other snow and terrain data that are more routinely available. Statistical models of this type

have been extensively used to estimate relationships between snow point measurements and physiography, though previous efforts were applied to manual SWE data sets of limited spatial coverage (Balk and Elder, 2000; Elder et al., 1998; Erickson et al., 2005; Fassnacht et al., 2003; López-Moreno and Nogués-Bravo, 2006; Molotch et al., 2005; Schneider and Molotch, 2016). At small scales (i.e. $< 10 \text{ km}^2$), dedicated sampling of headwater catchments has led to models that explain between 20% and 65% of the variability in snow depth based on physiographic variables at 30m resolution (Balk and Elder, 2000; Elder et al., 1998; Erxleben et al., 2002). Importantly, Erickson et al. (2005) found persistence in the topographic controls on snow depth distribution and successfully parameterized a multi-year model relating the physiographic variables of a small headwater catchment to annual peak snow depth by scaling the mean based on in situ measurements. Later studies have since confirmed an inter-annual consistency in snow depth distribution based on high resolution lidar measurements (Deems et al., 2008; Schirmer et al., 2011; Trujillo et al., 2009) and the inter-annual persistence of topographic controls on snow depth distribution (Grünwald et al., 2013; Revuelto et al., 2014). These previous works suggest that relationships between lidar snow depth measurements and topography may be useful for extending lidar measurements of snow in time.

The lidar measurements provide snow depth, and coincident density measurements or estimates are required to estimate SWE. However, snow depth measurements still capture the majority of the variability in SWE because snow depth varies an order of magnitude greater than density (Jonas et al., 2009; López-Moreno et al., 2013; Mizukami and Perica, 2008). Hence, we expect the results from the previous studies be relevant here, i.e. inter-annual consistency in SWE distribution will be similar to that of snow depth. Given the difficulty of extensively measuring density and SWE, operational SWE observation networks that use snow pillows to measure SWE have been used to relate physiography and SWE. In this regard, multiple studies have explained up to 82% of the variability in SWE based on physiographic variables (Fassnacht et al., 2003; Harshburger et al., 2010; Schneider and Molotch, 2016). These studies aimed to understand the processes controlling snow distribution and to apply this knowledge to interpolate point observations of SWE to $>1000 \text{ km}^2$ for a single point in time. The snow pillow networks, however, are constrained to flat sites in a relatively narrow elevation band below treeline. The spatio-temporal dataset of SWE from ASO, which covers the full range of physiographic variables present in a $1,175 \text{ km}^2$ watershed, provides an unprecedented opportunity to develop relationships between SWE and topography and test their persistence across several years.

Given that topographic variables are largely static in time, additional time-variant variables should be useful in the context of explaining the spatio-temporal distribution of SWE. Remotely sensed snow covered area (SCA) has long been recognized to provide information relevant to snowpack water storage and consequently expected summer streamflow (Cline et al., 1998; Good and Martinec, 1987; Martinec and Rango, 1981; Molotch and Margulis, 2008; Potts, 1937; 1944). Currently, SCA is commonly estimated from SWE in hydrologic models through a depletion curve parameterization in order to constrain melt production to the areal extent of snow cover (Anderson, 1973; Clark et al., 2011; Lawrence et al., 2011; Livneh et al., 2010; Luce and Tarboton, 2004; Niu et al., 2011). The utility of depletion curves to provide sub-grid information in physically-based modeling suggests that fSCA should provide additional information in statistical models of SWE distribution. The assumption of a consistent relationship between fSCA and SWE is predicated on the fact that SWE distribution is extremely heterogeneous over complex terrain and terrain features are progressively uncovered during the melt season. This process varies only slightly each year because of

similarities in the meteorology, e.g. wind direction that drive accumulation patterns and solar exposure that drives melt processes (Luce and Tarboton, 2004; Revuelto et al., 2016; Sturm and Wagner, 2010). Snow covered area is also relatively easy to measure due to the distinctive spectral signature of snow compared to soil, rock, and vegetation. In fact, photographic estimates of fSCA have been utilized for seven decades within hydrologic applications (Parsons and Castle, 1959; Potts, 1937; 1944) and today robust observations of fSCA can be obtained from variety of ground-based, aerial and satellite optical imagers (Bloschl et al., 1991; Dozier et al., 1981; Hall et al., 2001; Kirnbauer and Bloschl, 1994; König and Sturm, 1998; Painter et al., 2009; Rittger et al., 2013; Rosenthal and Dozier, 1996).

The repeat observations from ASO provide a unique dataset of concurrent SWE and fSCA over multiple years with which to develop robust statistical relationships between SWE, fSCA, and topography. Given that fSCA is widely observable from a variety of satellites, these relationships could then be used to estimate SWE for any date on which fSCA observations are available. Hence, the objective of this research is to use ASO-derived relationships between SWE (dependent variable) and fSCA and physiography (independent variables) to estimate SWE distribution for time periods when ASO data are not available. We aim to test how well statistical models of the relationship between SWE, fSCA and physiography transfer in time. We ask (1) Does fSCA improve statistical models of SWE distribution? (2) Can statistical models of SWE distribution be transferred directly from one year to another? (3) How can we determine which SWE distribution from the ASO record best represents a date of interest?

We present our SWE distribution modelling framework and show the utility of including the time-variant variable fSCA for improving the SWE distribution estimates. Next, we evaluate the impact of transferring models from one year to another. Lastly, we present a methodology for identifying which models of SWE distribution, from the ensemble of historical ASO acquisitions, best represents the SWE distribution for hypothetically unsampled dates of interest. We then discuss the results in the context of extending ASO to unsampled dates.

2 Site Description

We used a SWE dataset from the Tuolumne River basin in the Sierra Nevada mountains in California, USA (Fig. 1). The basin is 1,175 km² in area, consisting of 48% vegetation, 50% rock, 2% water, and small isolated areas with permanent snow/ice. The elevation range is 1127 m to 3965 m, encompassing 4 distinct ecological zones ranging from lower montane forest to alpine (NPS, 2016). The lower montane forest ranges from 1127 m to 1800 m elevation and consists of a diverse mix of coniferous and deciduous trees. The upper montane forest ranges from 1800 m to 2450 m elevation and primarily consists of coniferous species such as red fir (*Abies magnifica*) and lodgepole pine (*Pinus contorta*). Elevations from 2450 m to 2900 m are considered subalpine and consist of a mix of meadows and coniferous forest. The highest elevation band above 2900 m is an alpine zone that is devoid of tree cover and contains limited herbaceous vegetation. This alpine zone contains areas with large granitic features, talus slopes and boulder fields. Snowmelt from the basin runs off into the Hetch Hetchy reservoir, which is the main water supply for the City of San Francisco.

Analysis of SWE measurements from snow pillows show that historical mean peak SWE ranges from 0.3 m to 1.5 m with a mean of 0.8 m. Each of the study years was characterized by below average snowpack with 2014 and 2015 characterized as a severe dry snow drought (Harpold et al., 2017), experiencing only 36% and 35% of the

climatological mean peak SWE, respectively. The years 2013 and 2016 also experienced below average snowpack conditions, but less severely, with the data from the snow pillows reporting 62% and 71% of climatological peak SWE, respectively. Typically, minimum temperatures range from -12°C in winter to 3°C in summer and maximum temperatures range from 4°C in winter to 22°C in summer (Cristea et al., 2017).

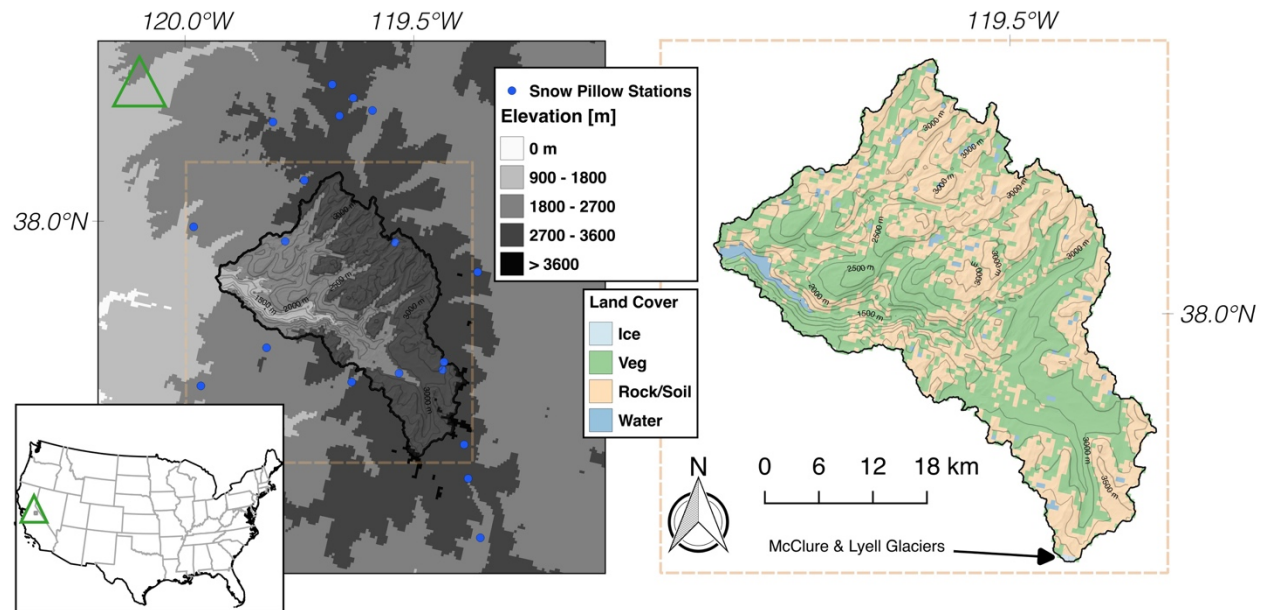


Figure 1. Elevation with snow pillows shown as blue dots (left) and land cover map of the Tuolumne Basin (right). The land cover data was provided by ASO and was derived from spectral information from summer snow-off flight. The snow pillows locations were obtained from the California Department of Water Resources. 250 m contour lines are shown on both maps.

3 Data Sources

We utilize the ASO dataset in the Tuolumne River Basin in the Sierra Nevada mountains of California. The ASO mission consists of airborne lidar in conjunction with a hyperspectral spectroradiometer (Painter et al., 2016). The dataset consists of 3 m snow depth maps for which snow-free areas are masked using spectral information from the spectroradiometer, 3 m vegetation height map and 50 m SWE maps. The dataset is distributed in the UTM zone 11 and WGS84 datum map projection system.

In order to conduct our analysis at a spatial scale that will ensure transferability to more widely available data, we mean-aggregated the 50 m SWE maps to 500 m. We chose the 500 m resolution because it is the scale for which commonly-used daily satellite fSCA products are available from the Moderate Resolution Imaging Spectroradiometer (MODIS) (Painter et al., 2009; Salomonson and Appel, 2004). Subsequently, we converted the 3 m snow depth maps to 501 m using mean aggregation and then bilinearly resampled to the 500 m SWE grid. We also used a binary aggregation of the 3 m snow depth maps to obtain 501 m fSCA maps, which were then resampled to 500 m by nearest neighbor to preserve snow free pixels. We used the Global Multi-resolution Terrain Elevation Data

2010 digital elevation model (data available from the U.S. Geological Survey at <https://lta.cr.usgs.gov/GMTED2010>) reprojected to the 500 m SWE grid to compute the physiographic predictor variables (Table 1).

Table 1. List of physiographic variables considered in the multiple linear regression to model SWE distribution. Source includes studies in which these variables have been used and the source of the algorithm, if applicable. Citations in the source column are by no means exclusive.

Variable	Units/Derivation Specifics	Source
UTM Northing	meters	Fassnacht et al. (2003)
UTM Easting	meters	Fassnacht et al. (2003)
elevation	meters	Elder et al., (1991, 1998); Balk and Elder (2000)
northness	$\sin(\text{slope}) \cdot \cos(\text{aspect})$; ranges 0-1; dimensionless	Fassnacht et al. (2003); Molotch et al. (2005)
eastness	$\sin(\text{slope}) \cdot \sin(\text{aspect})$; ranges 0-1; dimensionless	Fassnacht et al. (2003); Molotch et al. (2005)
topographic position index (TPI)	elevation difference of a pixel from the mean of the surrounding pixels using a 9x9 pixel window; meters	Revuelto et al. (2014); GDAL (2015)
vector ruggedness measure (VRM)	3-dimensional measure of the variation of slope and aspect in a 9x9 pixel window; not correlated with slope or aspect; ranges 0-1; dimensionless	Veitinger et al. (2015); Sappington et al. (2007); Conrad et al. (2015)
standard deviation of slope	standard deviation of slope in 7x7 window around each pixel; shown to detect changes in slope at multiple scales; radians	Marchand and Killingveit (2005); Lopez-Moreno et al. (2014); Grohman et al. (2007)
vegetation height	measured by ASO; used in place of forest canopy density from previous studies; meters	Molotch and Bales (2005, 2006); Painter et al. (2016)

The ASO flies approximately weekly from near peak SWE to the end of the melt season. As such, there were six flights in 2013, ten in 2014, eight in 2015, and eight in 2016. Only the final four flights of the 2016 season were available for this study resulting in a total of 28 SWE maps. Painter et al. (2016) report a mean absolute vertical snow depth error of <8 cm and a bias of <1 cm when compared with manually measured snow depths at the 15 × 15 m scale. Further details about the mission and processing can be found in Painter et al. (2016).

We also obtained daily SWE measurements from the 17 snow pillows operated by the California Department of Water Resources that are within 20 km of the Tuolumne watershed boundary. We chose 20 km from a range of 10 km to 50 km because it produced the best results. The stations range from 2000 m to 3250 m. We downloaded the adjusted SWE records, which have been manually quality controlled, for the 2013-2016 water years. No further adjustments were performed. The data can be downloaded from <http://cdec.water.ca.gov/>.

4 Methods

We use linear regression to model the distribution of SWE for every ASO flight. The explanatory variables we consider are ASO-observed fSCA and topographic variables previously used in the literature (Table 1). The topographic variables were directly computed from the 500 m digital elevation model with the exception of vegetation height which was derived from the 3 m ASO vegetation height by mean aggregating to 501 m and bilinearly resampling to 500 m. Of note, we use three different windowed variables (topographic position index (TPI), vector ruggedness index

(VRM), and standard deviation of slope); to the best of our knowledge these have not previously been used for resolutions larger than 25 m. Comparison with ASO SWE at 500 m shows mean correlations of 0.3, -0.26, and -0.31, respectively, and we consider these variables indicative of preferential deposition from orographic updraft (Dadic et al., 2010; Garvert et al., 2007; Lehning et al., 2008). The window sizes were chosen based on the maximum correlation between ASO SWE and the variable, where the marginal increase in correlation from the next smaller window size was greater than 10%. We tested each odd window size from 3x3 to 15x15 pixels which equate to 1.5 km to 7.5 km scale, respectively.

We present results from two models: 1. “PHV” is a multiple linear regression that consists only of physiographic variables as independent variables. This represents the traditional approach for estimating SWE distribution based on relationships with physiography; 2. “PHV-FSCA” is a multiple linear regression that includes both physiographic variables and fSCA as independent variables. We make these distinctions to demonstrate the utility of fSCA as a time-variant variable, which has not yet been explicitly explored for its utility in directly estimating the distribution of SWE. fSCA values including zero are used to fit the PHV-FSCA models. Regression estimates from both PHV and PHV-FSCA are masked to snow covered areas as observed by ASO. Once we illustrate the utility of the statistical models for characterizing ASO SWE distribution patterns for a given day, we then explore how these statistical models can be transferred to time periods without ASO observations. With regard to all statistical models, we report the squared Pearson correlation coefficient (r^2) as a measure of the relative spatial pattern between the modeled SWE distribution and ASO observed SWE distribution. We also report the mean absolute error as a percent of mean observed SWE (%MAE) as a measure of the accuracy of the modeled SWE distribution. Lastly, we report bias as a percent of mean observed SWE (%Bias) as a measure of the systematic over or under-prediction by the model.

4.1 SWE Models: Same Day

To examine the utility of fSCA as a predictor, we compared the SWE distributions modeled with PHV and PHV-FSCA using a split sampling strategy; these are known as *same-day models*. We randomly split the data for each date into a training (80%) and test (20%) dataset to evaluate overall model performance on this date. This insures that we are not evaluating the model with the same data used to create the model. Furthermore, this procedure is replicated 20 times to provide 20 different subsets with which to evaluate model performance; this is more robust than a single replication. More replications were computationally prohibitive. This split sample strategy is an important initial step in transferring ASO data in time as it is necessary to first show that fSCA and physiographic variables can be used to adequately model ASO-observed SWE on the date of acquisition. Once this is established, the transferability of the models in time can then be explored – as described in the next section.

4.2 SWE Models: Transferred in Time

We evaluated a second set of predictions whereby each date is modeled using all the data, i.e. not split, and then this model is used to predict SWE on dates that ASO flew in different years. In this manner, we simulate SWE on the date ASO flew using models from other years and then we use the ASO data on the date of interest strictly to evaluate the

model estimates of SWE. Hereafter, we refer to the date of the model (i.e. the date of the ASO observation for which the model is developed) as the *model date* and the date being predicted as the *transfer date*. This results in 28 models of SWE distribution for PHV and PHV-FSCA each because there are 28 ASO flights. Given our primary goal of estimating the SWE distribution for unsampled dates, we apply models developed for each ASO acquisition to all other dates except for dates within the same year as that in which the model was developed. For example, in 2013 there were a total of 6 ASO flights out of the total of 28 flights during the four-year study period. This leaves 22 flights from other years that can be used to develop statistical models of SWE that can be transferred to the dates in 2013. By conducting our model tests in this manner, we are robustly testing the transferability of models from a given *model date* with regard to simulating SWE distribution on a given *transfer date* in a hypothetical future year. Due to a different number of ASO observations in each year, the prediction ensemble size differs for each year. As noted above, for each date in 2013 there are 22 potential models. For each date in 2014 there are 18 potential models; for each date in 2015 there are 20 potential models; and for each date in 2016 there are 24 potential models. These models are referred to as *transferred models*, and for each *transfer date* we identify the *best model* from another year based on error statistics generated from the ASO data acquired on the *transfer date*. We refer to this model as the *best model*.

The ability of a model to transfer from the one date to another will vary based on how well the relationships between the dependent variable (SWE) and explanatory variables are captured and the similarity of the SWE distributions. Here we quantify the SWE similarity between dates using the mean absolute error (MAE) of SWE recorded at snow pillows on both dates within 20 km of the basin as shown in Figure 1; station data was not weighted by distance to the basin or elevation. For each *transfer date*, there is an ensemble of predictions from the *model dates* from the other years. Each of the *model dates* exhibit a similarity with the SWE distribution of the *transfer date*. In order to pick which model date exhibits the greatest similarity with the *transfer date* without having an ASO observation, we calculate the MAE of SWE at the snow pillows between each pair of model-transfer dates and select the *model date* with the lowest MAE. We compare the prediction performances from this model selection procedure (denoted *selected model*) with those of the *best models*. We recognize that a given SWE pattern from the snow pillows may correspond to multiple basin-wide SWE patterns 1, but given our objective of extending ASO observations to real-time applications, we must use other data that is available. Some discussion of other options is presented in the Discussion.

4.3 Statistical Model

The multiple linear regression models described above, i.e. PHV and PHV-FSCA, are based on a regularized regression model applied in an elastic net framework (Friedman et al., 2010). The benefit of a regularized regression over standard regression is that it reduces overfitting while permitting all theoretically relevant variables to be included, rather than removing potentially useful variables due to multicollinearity. Regularized regression increases the predictive ability of a model with multiple predictor variables by penalizing the objective function used to estimate the parameter set. The elastic net is an extension of ordinary least squares, which estimates parameter coefficients by minimizing the residual sum of squares (RSS) as the objective function (Eqn 1):

$$RSS = \sum_{i=1}^n \left(y_i - \sum_{j=1}^p \beta_j x_{ij} \right)^2 \quad \text{Eqn (1)}$$

where y_i is the response variable at the i^{th} observation, β_j is the coefficient for predictor variable j , and x_{ij} is predictor variable j at each observation i . The elastic net penalizes RSS by two different types of regularization techniques, known as L1 and L2, that have opposing properties (more on this below). In this regard, the elastic net estimates the regression parameters β by minimizing RSS in Eqn 2:

$$RSS = \sum_{i=1}^n \left(y_i - \beta_0 - \sum_{j=1}^p \beta_j x_{ij} \right)^2 + \lambda P_\alpha(\beta) \quad \text{Eqn (2)}$$

where

$$P_\alpha(\beta) = \sum_{j=1}^p \left[\frac{1}{2} (1 - \alpha) \beta_j^2 + \alpha |\beta_j| \right] \quad \text{Eqn (3)}$$

β_0 is the intercept, λ controls the magnitude of the penalty, and α changes the relative influences of the L1 and L2 regularizations. In practice, this shrinks the coefficient values towards zero for variables exhibiting multicollinearity and for predictors with low explanatory power. Penalized coefficients have lower variance and therefore variables can be selected without resorting to a discrete selection procedure, e.g. a p-value threshold such as in step-wise regression. Consequently, resulting parameter sets are more robust predictors for independent data (Zou and Hastie, 2005).

The elastic net has two tuning parameters, λ and α , which are determined through cross validation. When $\alpha=1$, the penalty is composed completely of the L1 penalty and commonly known as Lasso regression. When $\alpha=0$, the penalty is composed completely of the L2 penalty and is commonly known as Ridge regression. The advantage of the elastic net is that α can range between 0 and 1 and therefore inherits the properties of both L1 and L2 regularization. L1 regularization is commonly used for model selection because predictor coefficients can be shrunk to zero and effectively removed from the model. However, in the presence of correlated predictor variables, one predictor variable would be randomly selected while the others are removed. This can result in decreased predictive performance since variables with some explanatory power are no longer in the model. With L2 regularization, regression coefficients will shrink towards zero but with an asymptote at zero. This is the preferred type of regularization in the presence of multicollinearity because all variables would remain in the model but with smaller coefficients. For further details, we direct the reader to Zou and Hastie (2005) and Hastie et al. (2009).

We do not directly treat spatial correlation in our models due to the large computational demands of fitting the covariance function for ~4000 pixels for 28 dates. Neglecting spatial correlation is another potential source for regression coefficients to be overfit and consequently we do not interpret them for physical meaning (Cressie, 1993;

Erickson et al., 2005). Nonetheless, we show utility with our methods without addressing spatial correlation and expect the results presented herein would improve if spatial correlation were explicitly treated (Carroll and Cressie, 1997).

5 Results

5.1 SWE Models: Same Day

Table 2 shows that PHV-FSCA outperforms PHV in all metrics in all years except %Bias (where both models exhibit close to 0 %Bias, as expected from a regression). The model PHV-FSCA explains on average between 80% and 85% of the variance in SWE distribution in any given year whereas PHV only explains between 56% and 67%. We similarly see improvement in %MAE where PHV-FSCA exhibits mean annual %MAE between 26% and 40% compared with PHV which yields mean annual %MAE between 47% and 66%. In summary, we note a substantial improvement in r^2 and %MAE for distributing SWE when fSCA is included as an additional variable.

Table 2. Mean prediction performance for PHV and PHV-FSCA from each observation date using a split-sampling approach.

	PHV			PHV-FSCA		
	r^2	%MAE	%Bias	r^2	%MAE	%Bias
2013	0.56	66	1	0.83	33	0
2014	0.67	47	2	0.85	26	1
2015	0.58	59	-1	0.82	32	1
2016	0.61	65	4	0.80	40	2
Mean	0.61	57	1	0.83	31	1

5.2 SWE Models: Transferred in Time

Figure 2 shows March 23, 2014 as an example transfer date that was predicted using a PHV-FSCA model from May 25, 2013. Overall, we see similar spatial trends between the observed and modeled SWE distributions, but we see lighter colors in the observed map indicating higher SWE. The mean observed SWE is 0.21 m compared to 0.22 m modeled. The range of observed SWE is 0-0.67 m while the modeled SWE ranges from 0-0.38 m. The standard deviations of observed and modeled SWE are 0.14 m and 0.12 m, respectively. The difference map shows large areas of agreement to within 0.05 m SWE and a qualitative comparison with Figure 1 suggests these are mainly forested areas. We see areas of under prediction (red) mostly above tree line in the north and southern tip, and areas of over prediction (blue) below tree line in the south. These errors correspond to the steepest slopes, which may be an effect of coarsening the data to 500 m. The snow extent is very similar between the modeled SWE and observed SWE because only areas observed to have fSCA greater than 0 were predicted.

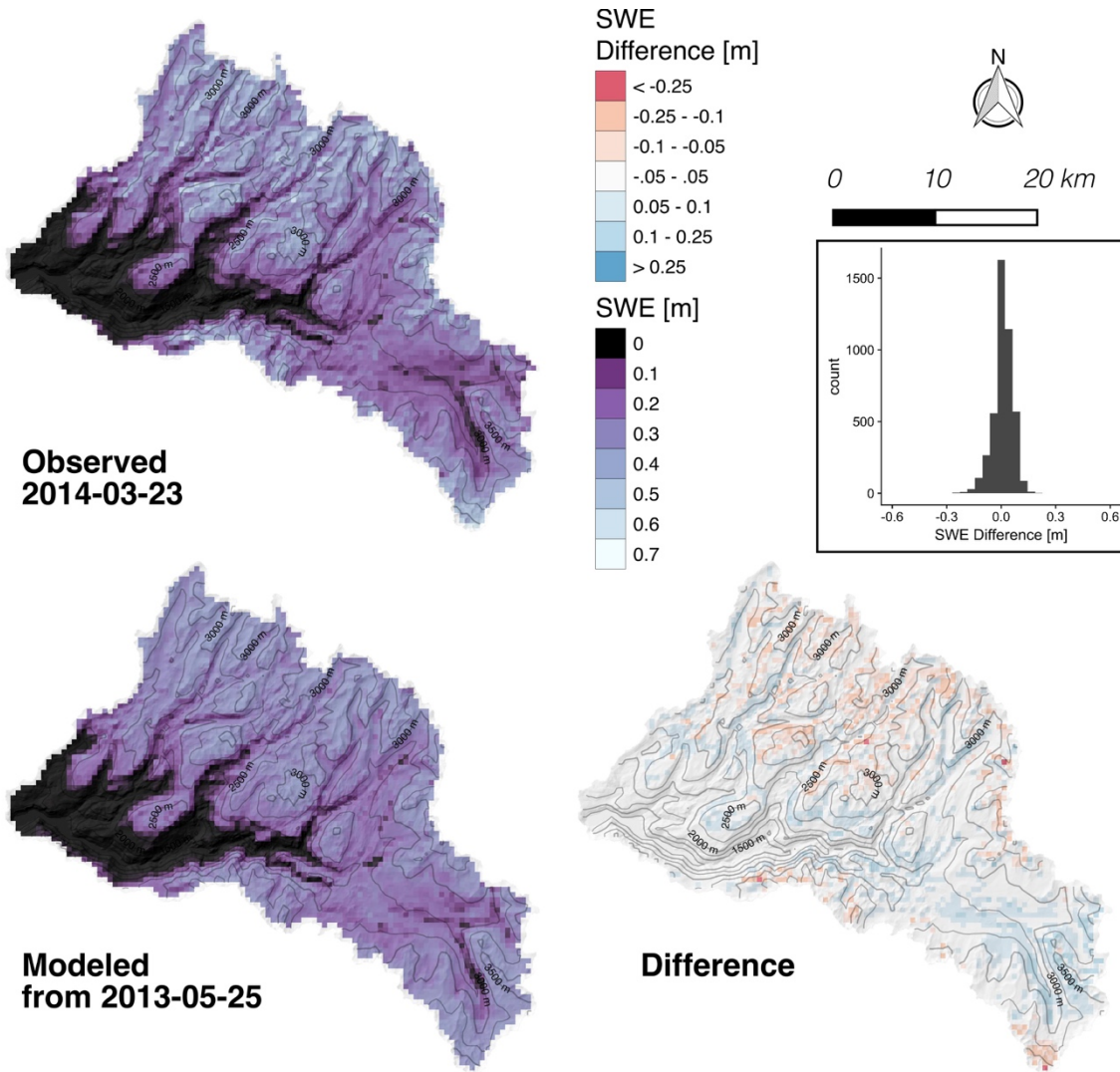


Figure 2. An example of SWE distribution from 2014-03-23. Observed SWE (top left); modeled SWE using PHV-FSCA (bottom left); the difference, modeled SWE – observed SWE (bottom right). A shaded relief and 250 m contours are used to highlight the topography. A histogram of the differences (top right).

Figure 3 shows the range of r^2 for *transferred models* for PHV and PHV-FSCA on each date based on models created in other years. Additionally, we highlight the *best model* performance for each transfer date by a diamond. We observe unanimous improvement across all dates with PHV-FSCA compared to PHV, except for April 9, 2015 where PHV yielded 0.01 higher r^2 . PHV-FSCA yields the highest mean best r^2 of 0.83 (mean of diamonds) compared to PHV with a mean best r^2 of 0.61. We also observe a notable decrease in r^2 for PHV towards the end of the season while PHV-FSCA exhibit a consistent r^2 . The standard deviation of r^2 for PHV is 0.13 and for PHV-FSCA it is 0.05.

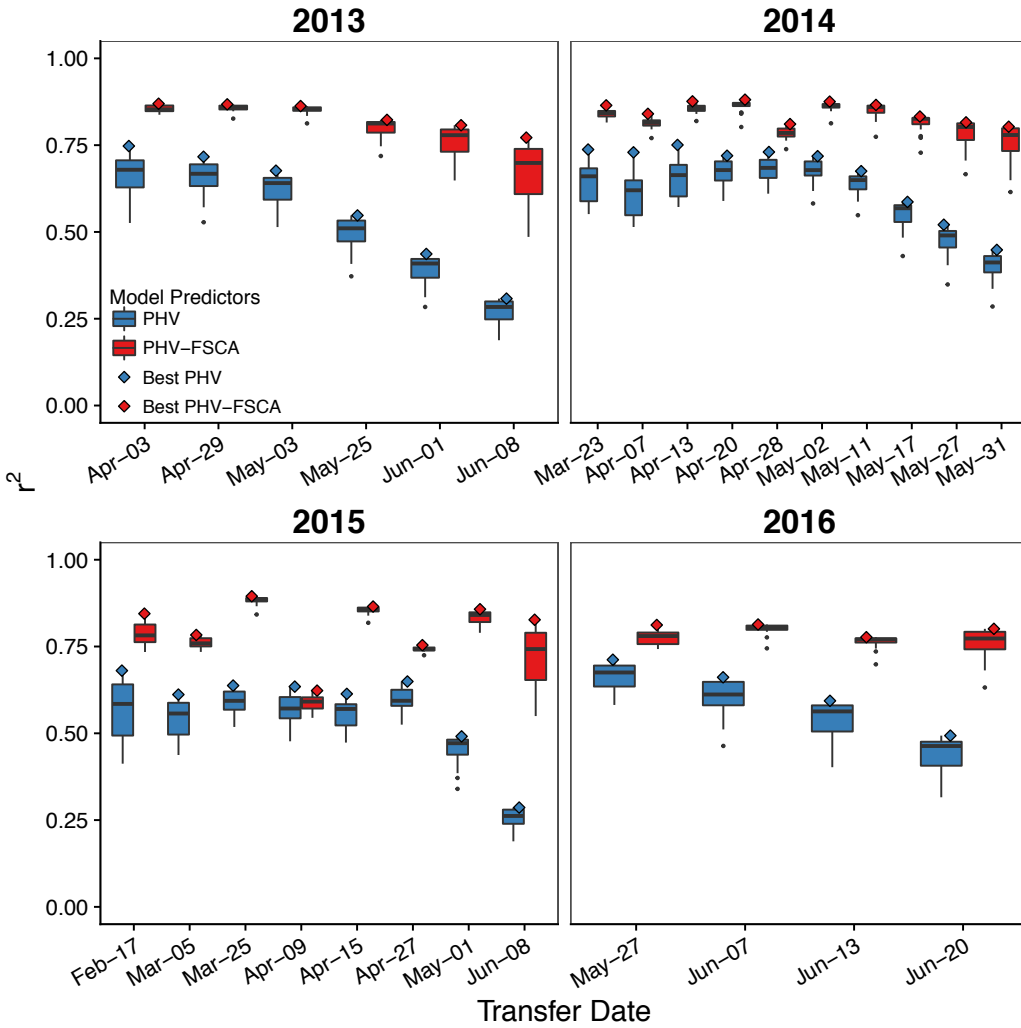


Figure 3. The range of r^2 for each simulation date from the *transferred models*. The diamond highlights the *best model* for each *transfer date*. The boxplots represent the interquartile range with vertical lines to denote the 5th and 95th percentiles. Black dots are outliers.

Figure 4 also clearly shows PHV-FSCA *transferred models* to exhibit better, i.e. lower, %MAE compared to PHV. April 9, 2015 is a notable exception where PHV exhibits the *best transferred model*. The mean best %MAE (mean of diamonds) for PHV-FSCA is 33% while the mean best %MAE for PHV is 60%. Particularly obvious in these panels is the upward distribution shift and larger range for PHV later in the season compared to only a minimal increase in %MAE for PHV-FSCA. The standard deviations of the best %MAE are 9% for PHV-FSCA and 25% for PHV.

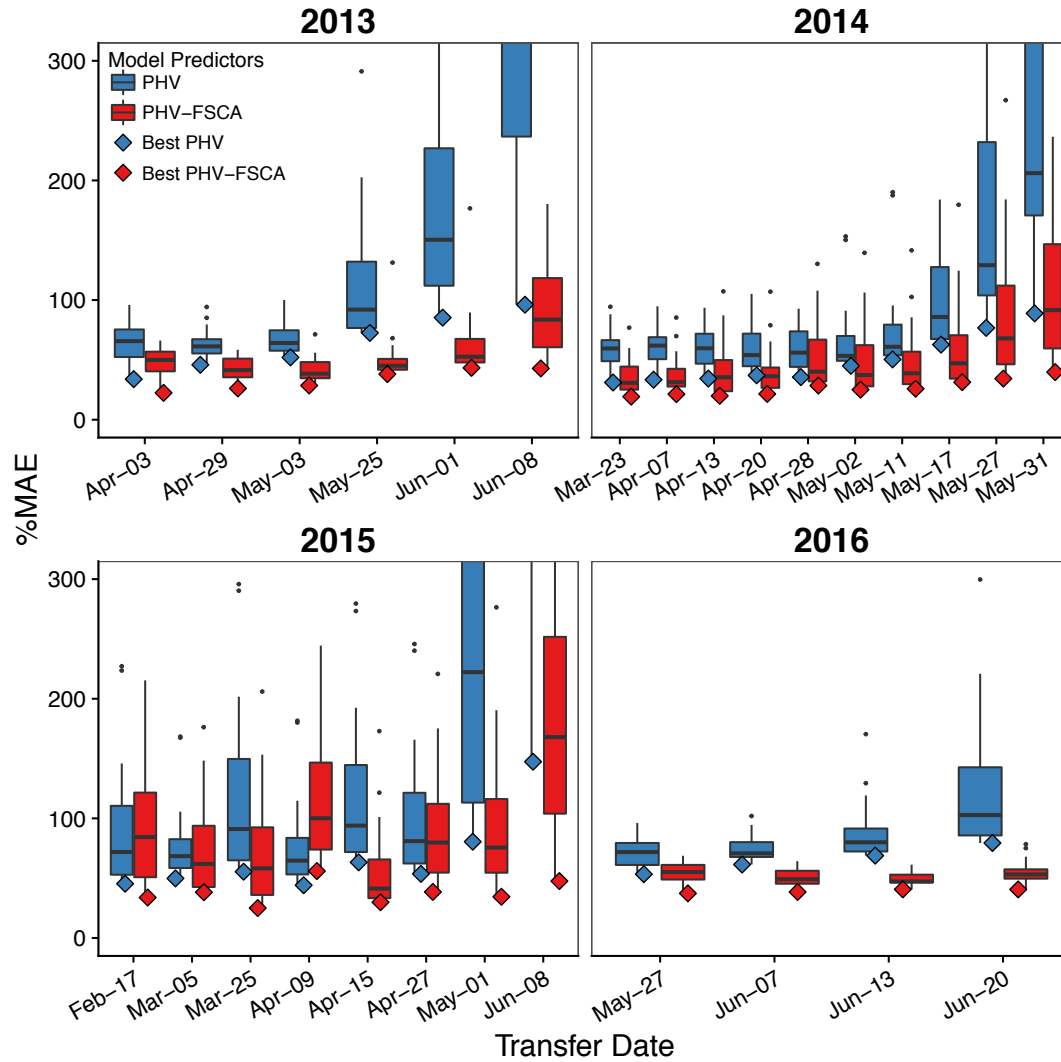


Figure 4. The range of %MAE prediction errors for each transfer date from the transferred models. The diamond highlights the best model for each transfer date. The y-axis is limited for clarity. The boxplots represent the interquartile range with vertical lines to denote the 5th and 95th percentiles. Black dots are outliers.

Figure 5 shows that the *best transferred models* (diamonds) for all models exhibit close to zero bias. The mean best %Bias for PHV is 1% and for PHV-FSCA it is 1%. However, we note that the variability in %Bias increases more dramatically at the end of the season, especially for PHV. The standard deviations of the best (i.e. lowest) %Bias for PHV and PHV-FSCA are 15% and 7%, respectively.

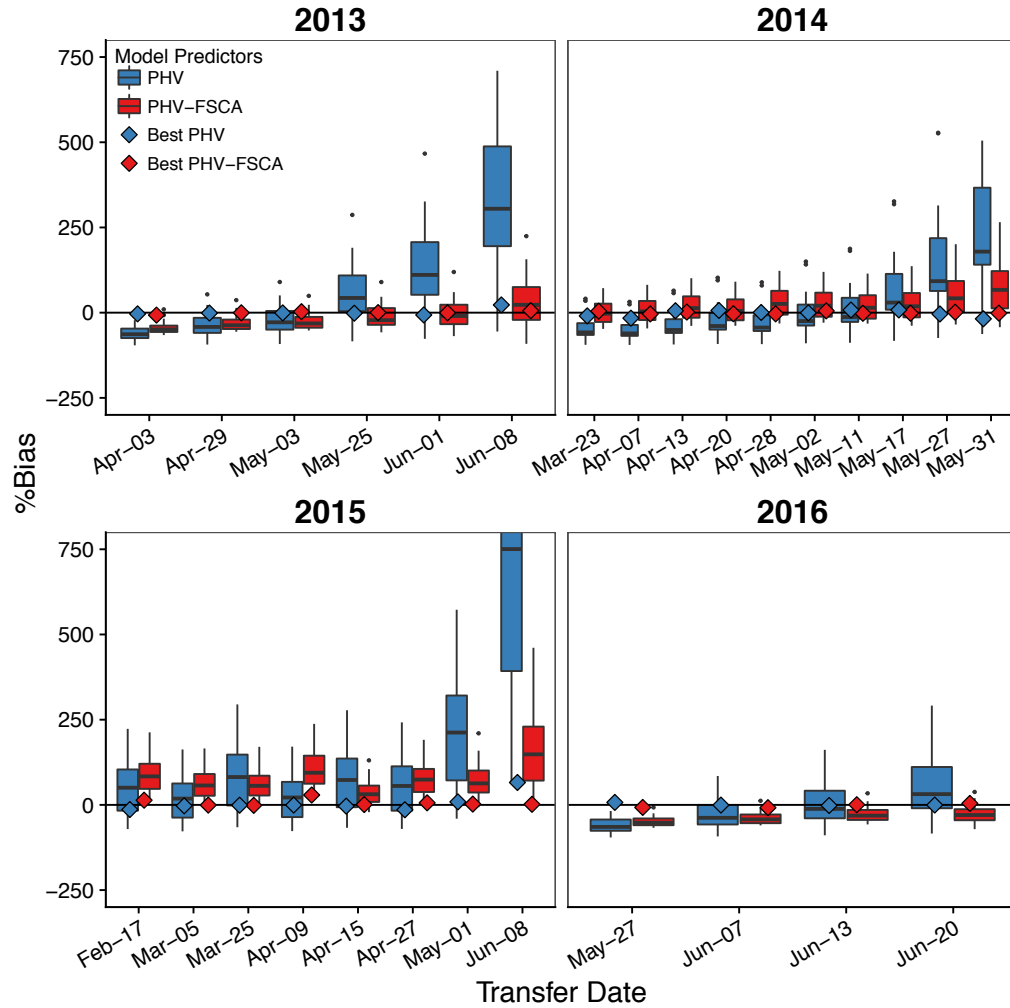


Figure 5. The range of %Bias prediction errors for each transfer date from the transferred models. The diamond highlights the best model for each transfer date. The y-axis is limited for clarity. The boxplots represent the interquartile range with vertical lines to denote the 5th and 95th percentiles. Black dots are outliers.

Following the demonstration of near unanimous improvement with fSCA as a predictor variable, we compare just the *best transferred models* of PHV-FSCA presented in Figs. 3, 4, 5 with the split-sample models of PHV-FSCA from the previous section, to assess the performance degradation one would expect due to transferring a model between years. We observe that PHV-FSCA models can be transferred to another year with little degradation in performance (Table 3). The yearly r^2 of the *best transferred model* are always within 1% of the *split sample model* and, on average, explains the same amount of variance in SWE distribution. The yearly mean %MAE of the *transferred model* is always within 5% of the *same-day model* with the mean 2% higher. The yearly mean magnitude of %Bias is actually lower, i.e. better, in 2014 with the *best transferred model* compared to the *same-day model*, and the overall mean is the same.

Table 3. Mean model performance comparison with PHV-FSCA for the split sample model and the best transferred model for each simulation date.

	Same Day Model			Best Transferred Model		
	r^2	%MAE	%Bias	r^2	%MAE	%Bias
2013	0.83	33	0	0.83	34	0
2014	0.85	27	1	0.85	27	0
2015	0.82	33	1	0.81	38	6
2016	0.80	40	2	0.8	39	-3
Mean	0.83	31	1	0.83	33	1

5.3 Evaluating the Selected Model Performance

Table 4 summarizes and compares the yearly mean statistics from PHV-FSCA for the *best models* and the *selected models* (i.e. those chosen based on snow pillow similarity) transferred from another year. The model selection procedure results in similar yearly r^2 to the *best models* but increases in both %MAE and %Bias are apparent with the *selected models*. Compared to the *best models*, yearly mean %MAE for *selected models* increases between 4% and 17% and yearly absolute %Bias increases between 2% and 34%. The years 2013, 2014, and 2015 yielded increases in %MAE of 17%, 16%, and 16%, respectively for *selected* versus *best models*. In 2016 selected model %MAE exhibited an increase of only 4%. The absolute %Bias increases 2% in 2013, 7% in 2014, 34% in 2015, and 24% in 2016 for *selected* versus *best models*.

Table 4. Yearly and overall prediction errors of PHV-FSCA for best transferred models and the selected models. Best transferred model errors involved fitting a model to all the data on each date and using these models to predict SWE on dates in other years. Only the best model date-simulation date pair is considered. The selected model errors are derived from the same ensemble of model date-simulation date pairs, but the model is selected based on the pillow SWE similarity described in the text.

	Best Transferred Model			Selected Model		
	r^2	%MAE	%Bias	r^2	%MAE	%Bias
2013	0.83	34	0	0.82	51	2
2014	0.85	27	0	0.82	43	7
2015	0.81	38	6	0.79	54	40
2016	0.8	39	-3	0.79	43	-27
Mean	0.83	33	1	0.81	48	11

Figure 6 shows the difference for each *transfer date* between the errors of the *best models* (diamonds in Figs. 3, 4, 5) and the errors of the *selected models* (these are shown in Fig. 7). We focus on %MAE and %Bias from PHV-FSCA only because r^2 showed generally consistent performance for a given transfer date (Table 4; comparatively small vertical range of the red boxplots in Fig. 3 compared with Figs. 4 and 5).

The mean difference in %MAE between the *selected* and *best models* is 15% and the *selected models* exhibited the same %MAE as the *best model* on two dates (Fig. 6a). The range in performance difference is between 0% and 43% with a mean of 15% and median of 12%. The differences in %MAE were generally lowest in 2016 with a mean of 4% and standard deviation of 5%. In contrast, 2013, 2014, and 2015 exhibited both higher mean differences (18%, 17%, and 16%, respectively) and higher standard deviations in %MAE (13%, 7%, and 13%, respectively).

The *best model* had a lower absolute magnitude %Bias of between 0% and 67% with a mean of 30% and median of 29%. The selected model was the same as the *best model* on one date (Fig. 6b). The yearly mean difference in error was consistently higher for %Bias than %MAE, with means of 27% in 2013, 32% in 2014, 33% in 2015, and 21% in 2016. The standard deviation in the error difference was lowest in 2014 (8%) compared to 14% in 2013, 20% in 2015, and 11% in 2016.

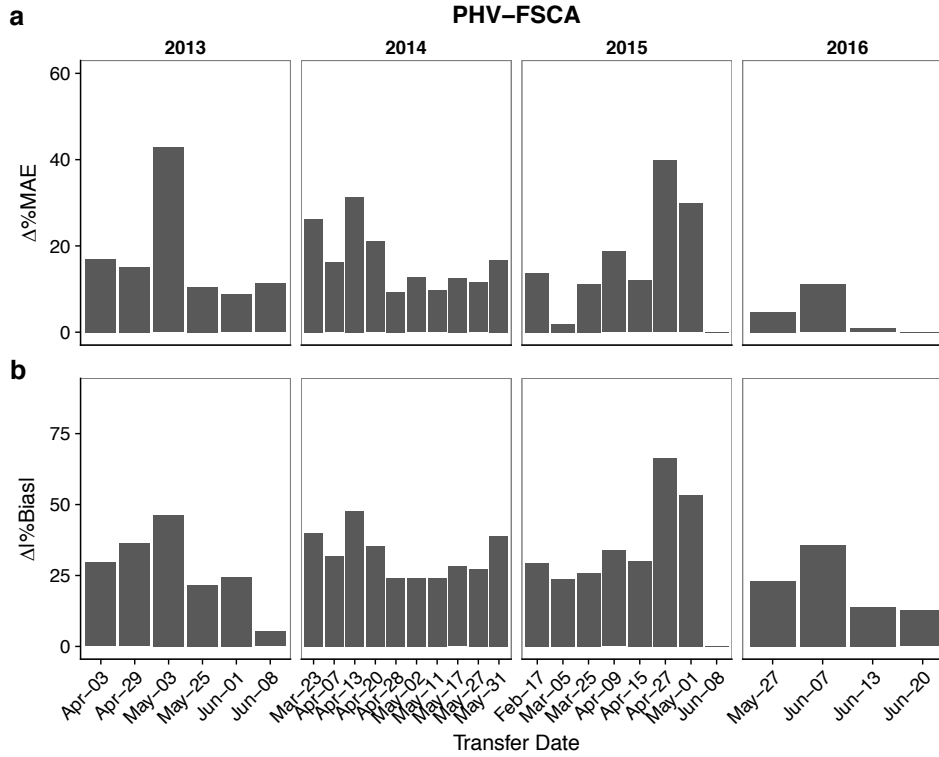


Figure 6. The increase in prediction error for %MAE (a) and %Bias (b) between the *best model* and the *selected model*.

We evaluate the prediction errors from different model years to see if there are any systematic differences in the predictions generated; i.e. do some years yield better predictions of other years? This allows us to determine how sensitive predictions for transfer dates will be given the existing ensemble of observations. In this context, we note distinct differences in the predictive ability of models from different years, which has important implications for the ability of a model to transfer in time.

Figure 7a shows that, on average, models *from* 2015 produced the lowest %MAE and models from 2016 produce predictions with the largest %MAE. The mean %MAE in 2016 is 113% compared to 75% with 2013 models, 59% with 2014 models and 47% with 2015 models. We observe consistency in a year's ability to predict another year relative to the overall distribution, i.e. the colored dots are typically clustered within the range of the boxplots. We also note in 2016 that the *best models* always came from 2013, but in 2013 the *best models* only came from 2016 for the first three flights. In 2014, the bulk of the models around the median performance were from 2015 and vice-versa in 2015. In these two years, the poorest predictions were from 2013 and 2016.

Figure 7b show that models *from* 2016 also produce the largest %Bias with a mean of 94% compared with 56% from 2013, 11% from 2014, and -30% from 2015. We again see consistency in the location of the colored dots relative to the boxplots, thus suggesting models from certain years will consistently estimate the SWE distribution of certain other years better. Similar to the %MAE results, 2013 produces the lowest %Bias in 2016, but in 2013 the inverse is only true for the first three flights as the distribution shifts up.

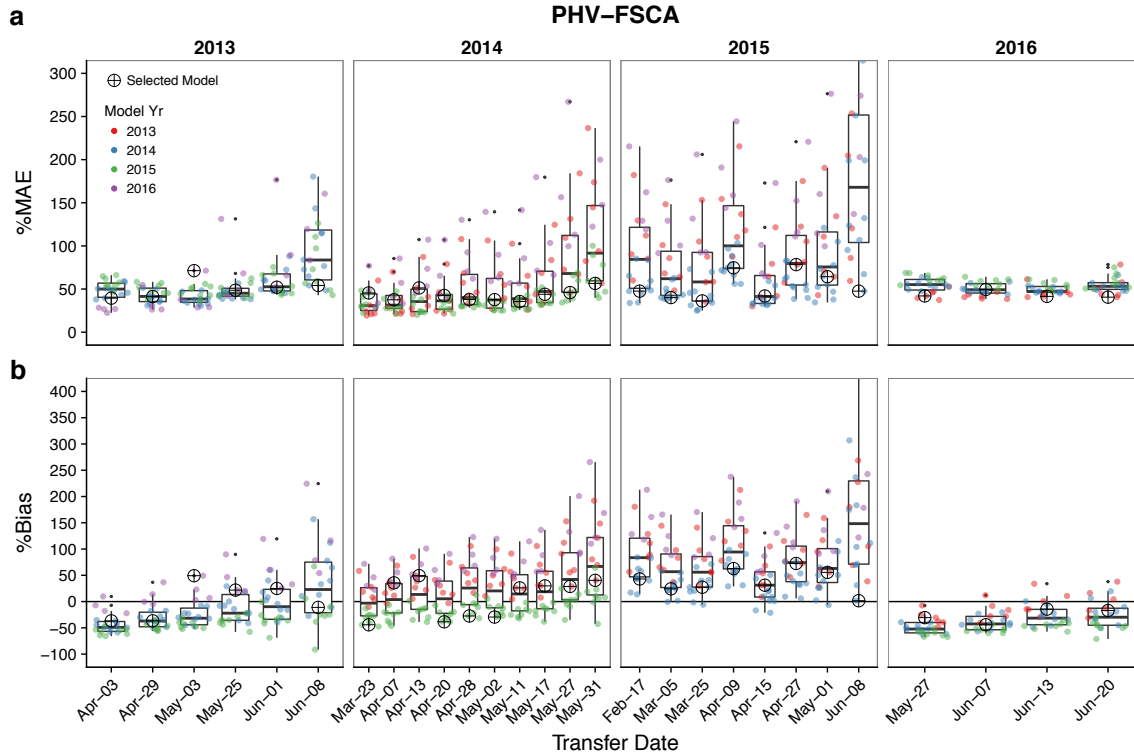


Figure 7. The prediction errors for PHV-FSCA for each date; %MAE (a) and %Bias (b). The colored dots are the prediction errors coded by model year and jittered to prevent over plotting. The symbol ‘⊕’ represents the selected model. The boxplots represent the entire distribution of prediction errors for each date. The boxes represent the interquartile range with vertical bars for the 5th and 95th percentiles. Small black dots are statistical outliers.

6 Discussion

6.1 SWE Distribution Modeling

The relationship between snow covered area and SWE is well established as evident by the common use of depletion curves in hydrologic modeling (Anderson, 1973; Clark et al., 2011; Liston, 1999; Luce et al., 1999). We invert the idea of the depletion curve in this study by using the spatial distribution of fSCA to predict the spatial distribution of SWE. The basis for this approach is relatively well established given that fSCA is sensitive to topographic complexity and the spatial distribution of SWE (Cristea et al., 2017; Donald et al., 1995; Fassnacht et al., 2016; Niu and Yang, 2007; Walters et al., 2014). We extend the concept of linking fSCA with topography from these previous works to estimating SWE distribution. In this regard, model performance consistently improved when fSCA was used as a predictor, with an average %MAE decrease from 60% with PHV to 33% with PHV-FSCA. The utility of fSCA as an

explainer of SWE distribution is not an unprecedented result. König and Sturm (1998) showed that in situ measurements of SWE were correlated with fSCA from aerial photographs. In addition, Marchand et al. (2005) suggested that the sub-grid standard deviation of physiography could improve regression models of SWE distribution because it accounts for sub-grid snow depth variability. Remotely sensed fSCA provides a means of capturing this sub-grid variability in SWE without requiring higher resolution data to compute the variance of physiography for each pixel.

The statistics for the selected PHV-FSCA model reported in this study compare favorably to SWE distribution statistics reported previously. Headwater catchment scale studies, based on intensive field data, have been able to achieve r^2 values from as low as 0.18 to as high as 0.65 (Balk and Elder, 2000; Elder et al., 1991; 1998; Erxleben et al., 2002; López-Moreno and Nogués-Bravo, 2006; Molotch and Bales, 2005) compared to the mean r^2 of 0.81 for the *selected models* in this study. The results presented herein also compare favorably with larger scale studies (i.e. $> 1000 \text{ km}^2$) of snow distribution. Fassnacht et al. (2003) reported average yearly RMSE between 0.12 and 0.16 m and 0 m bias when cross-validated with snow pillows. Harshburger et al. (2010) reported an average r^2 of 0.82 and RMSE of 0.05 m when cross-validated with snow pillows. Schneider and Molotch (2016) reported a mean RMSE of 0.23 m and %Bias of 0.8% from snow surveys in the Upper Colorado River Basin. This is compared to a mean RMSE of 0.08 m and mean %Bias of 11% for the selected model in this study. The favorable error statistics reported here are even more encouraging when considering the differences in evaluation methods of these previous studies. In this regard, the error values reported here are quite robust in that we compare against spatially explicit observations over relatively large spatial scales (i.e. $> 1000 \text{ km}^2$). In contrast, the aforementioned works were evaluated against relatively sparse observations in relatively homogenous, flat, forested environments (Fassnacht et al., 2003; Harshburger et al., 2010; Schneider and Molotch, 2016).

Bair et al. (2016) compared a retrospective SWE reconstruction to the same ASO observations (2013-2015) and reported yearly mean %MAE between 20% and 31% and yearly mean %Bias between -11% and 10%. These yearly statistics are better than those reported in this study (Tables 3, 4), but are the result of a much more complicated energy balance model that can only be run after the snow has disappeared. The selected model in this study is a simple linear regression that can be applied in real-time, thus we consider our results valuable for applications where real-time estimates of SWE distribution are needed. In this regard, we compare our selected model results to SWE estimates from the U.S. National Weather Service's operational Snow Data Assimilation System (SNODAS). SNODAS produces spatially distributed SWE estimates for the coterminous United States at 1 km by assimilating a physically based model with snow pillow observations and remotely sensed snow covered area. The SWE product from SNODAS is the only high-resolution, gridded SWE product available at a daily time step for the continental United States and is available from <http://nsidc.org> (Barrett, 2003). Previous work has shown the physically based model to perform well at the point scale (Rutter et al., 2008) but suffer in alpine zones because it does not consider wind redistribution (Clow et al., 2012). In our own analysis, the yearly mean r^2 between ASO and SNODAS ranges from 0.04 in 2016 to 0.36 in 2015 with a mean of 0.17. The yearly mean %MAE ranges from 120% in 2014 to 274% in 2013 with a mean of 199%. The yearly mean %Bias ranges from -10% in 2016 to 236% in 2015. In comparison to the PHV-FSCA *selected model* in Table 4, SNODAS exhibits a mean %MAE 4 times greater than that of PHV-FSCA and a mean

%Bias 8 times higher than PHV-FSCA. Both models poorly predicted the anomalous conditions in 2015, which experienced high rain fraction and ephemeral snowpacks at low to mid elevations. While it is clear that the errors with PHV-FSCA are considerably lower than with SNODAS overall, SNODAS is a complex system that attempts to capture the snow dynamics across the entire United States compared with PHV-FSCA which was trained using a very specialized data set in the study region.

We also show that SWE distributions can be related to fSCA and physiography in one year and applied to another year. The performance of PHV-FSCA was quite similar when applied to the date at which the model was trained (i.e. *same-day models* with a split sample) versus applying the model to other years (i.e. *transferred models*), as evidenced by minimal decrease in prediction skill and minimal increase in prediction error when we compare *same-day models* with the *best transferred models*. Recall that the *same-day model* was trained and tested on the same day and the *transferred model* was trained in a different year from which the model was applied, yet the mean r^2 in the *same-day* is equivalent to that of the *best transferred model* (Table 3). Moreover, the average %MAE of the *best transferred model* exhibits only a 2% difference from the *same-day model* and the mean %Bias exhibits no difference. Thus, if we are able to identify the *best model* for a given date of interest we would see minimal degradation in predictive ability relative to a model derived from data acquired on the date of interest. However, we see significant differences in predictive ability from models of certain years (Fig. 7), which suggests that relationships between SWE and physiography are only similar between specific years, not as uniformly as put forth by previous studies (Erickson et al., 2005; Grünewald et al., 2013). Also, it is unclear as to the impact of climate non-stationarity with respect to the ability to transfer models to future years. Even so, for each year in this dataset there exists a corresponding year from which accurate predictions can be made.

The benefits of using fSCA as a predictor variable in the *transferred models* are particularly large at the end of the season when the errors are highest (Figs. 3, 4, 5). For the last 2 dates of each year, the average difference in %MAE between the best PHV model and best PHV-FSCA model was 50% compared to an average difference of 18% for the other dates. The improvements seen by including fSCA as a predictor are noteworthy because the ensemble of models trained using ASO observations could then be applied using remotely sensed fSCA from satellites, and recent advances in downscaling fSCA may further improve SWE estimates at the end of the melt season when only small patches of snow persist (Cristea et al., 2017; Li et al., 2015; Walters et al., 2014). Nonetheless, the degree to which satellite-based fSCA will improve model performance toward the end of the snowmelt season will be partially dictated by the accuracy of the fSCA data, which is subject to increasing uncertainty at low fSCA values and with downscaling (Painter et al., 2009; Rittger et al., 2013). Optical fSCA products such as MODSCAG also suffer in forested areas since snow cover is occluded by the canopy (Raleigh et al., 2013; Rittger et al., 2013). A viewable gap fraction correction is typically used to extrapolate fSCA to the occluded portions of a pixel by assuming that fSCA is the same under the canopy as it is in canopy gaps (Molotch and Margulis, 2008), and future studies should evaluate the sensitivity of PHV-FSCA to this assumption. Cloud cover can also obscure a satellite's view of the snow and therefore making it difficult to estimate the snow extent. However, Slater et al. (2013) showed that gaps of 5 or more consecutive days are rare with MODIS, thus suggesting that weekly estimates of SWE would be feasible. Lastly, omission and commission errors of cloud identification can provide erroneous estimates of fSCA although Parajka and Blöschl

(2008) report an overall filtering accuracy of 96% in the Alps. Nonetheless, this is still an active area of research (Dozier et al., 2008; Parajka and Bloeschl, 2008; Rittger et al., 2013; Xia et al., 2012).

6.2 Considerations for Extending the ASO Record

The value of ASO during the year flown is significant for water management because it provides high resolution SWE information with low uncertainty compared to traditional estimation methods and therefore facilitates more accurate water supply forecasts. The work presented here provides a first step in realizing the value of ASO subsequent to active operations. We find that the number of flights within a year affects the mean and variance of the predictions in other years by <1%; this was quantified by iteratively selecting between 1 and the number of observations in a given year 100 times and assessing the change in error. In other words, a greater breadth of value can be derived by flying ASO once per year for 10 years as opposed to 10 times in a single year.

One might also consider the value of a single flight each year for estimating SWE distribution on other dates in the same year and in this case we found the mean r^2 to be 0.82, %MAE to be 39%, and %Bias to be 7% when considering the best model for each date. These values are similar to the yearly values from the *best transferred model* from other years (Tables 3, 4), which supports the prior assertion that the good or equivalent performance of models from other years suggests a strong degree of persistence in snow patterns. We note the positive %Bias and suggest that this perhaps should not come as a surprise since we only used prior flights for the same year, which measured deeper snowpacks and greater fSCA than those modeled; ASO flights typically start around peak SWE. Future work should identify the importance of the fSCA state for transferring a model, and whether an ASO flight in the accumulation season might yield better results.

It is clear from our results that flights in one year do not necessarily transfer well to another year, e.g. 2016 to 2014 and 2016 to 2015 (Fig. 7). The model selection procedure relies on operational snow pillows to identify similar patterns of SWE between historical dates (i.e. model dates) and the date of interest (i.e. transfer dates). The relative homogeneity of these stations may have contributed to the general inability of these stations to select the best historical date for a given date of interest because distinct basin-wide SWE patterns may correspond to similar patterns at the snow pillows. It is well established that these snow pillows may not adequately represent the SWE of the surrounding terrain (Meromy et al., 2012; Molotch and Bales, 2006; Rice et al., 2011) but they provide the only source of real-time SWE information. However, the minimal degradation in prediction performance when considering the *best transferred model* motivates improvements for identifying the dates from the past with the most similar SWE distribution. As shown here, if these dates can be identified, the SWE can be modeled at accuracy levels that are equivalent to models generated from ASO data collected on the date of interest. We also tested the similarity in remotely sensed fSCA as a method for identifying the historical date with the most similar SWE distribution to the date of interest. We found that anomalous SWE and fSCA distributions make this method less robust than using snow pillow data. However, a completely remote-sensing based approach would be useful in data sparse regions where ground stations do not exist. A potentially robust remote-sensing based method could be to track fSCA through time and select a similar SWE distribution based on the trajectory of fSCA rather than a single snapshot of fSCA. It is also important to note that flying ASO during a year with an anomalously low snowpack such as in 2015 in California does

not necessarily reduce the predictive capacity of models for future years. In our case, 2015 provided useful estimates of SWE distribution in all the other years, including 2016, even though the models from the relatively wet year of 2016 did not transfer well to the very dry year of 2015 (Fig. 7).

Intuitively, it is not surprising that the models from 2016 did not transfer to other years because there was much more snow than in 2014 and 2015, which were very low snow years. Less intuitive, however, is why the inverse worked well, i.e. the models from 2014 and 2015 did transfer relatively well to 2016. In this regard, we see lower mean fSCA in 2016 for the same mean SWE in 2015 in the ASO data. This means that for the same mean SWE, there are deeper pockets of snow covering a smaller area remaining at the end of a higher snow year (i.e. 2016) than a lower snow year (i.e. 2015). Therefore, we would expect the relationships between topographic variables and SWE to become increasingly disparate from the underlying terrain with a deeper snow accumulation. Thus, the regression coefficients derived from years with deeper snowpacks do not adequately represent relationships found during years with shallow snowpacks. However, this does not mean that the model from the last date of the season (which is also a shallow snowpack) transfers well because this SWE distribution still largely represents the dominant spatial patterns from the peak SWE distribution (Egli and Jonas, 2009; Liston, 1999; Luce et al., 1999).

7 Conclusion

We estimated the relationships between SWE, physiography, and fSCA from ASO data. Our results show that fSCA information strongly improves statistical SWE models, and these models can be reliably transferred directly from one year to another due to strong persistence in snow accumulation and melt patterns. We estimate SWE in years beyond the ASO observation record with a mean r^2 of .83, mean %MAE of 33%, and mean %Bias of 1%. The relationships transfer robustly in time with no degradation in r^2 or %Bias and only 2% in %MAE when comparing predictions between models fit on the same day and the best models from a different year. Models with fSCA as a predictor transfer better than those without, and we suggest that the inclusion of fSCA provides information with regard to the variability of the SWE resulting from different accumulation and melt dynamics due to differences in terrain roughness. The availability of satellite images of fSCA thus can facilitate the transfer of modeled relationships based on ASO observations to dates when no airborne snow depth measurements exist. The crux of this approach is in selecting the model to transfer. We offer a method with which to select a model from another year based on the similarity in SWE distribution at existing snow pillows in the area. Comparison of the best predictions and the selected predictions results in a mild decrease in r^2 (0.02) and moderate increases in %MAE (15%) and %Bias (10%). The results motivate further refinement in the technique used to select the *best model* because if these dates can be identified then SWE can be modeled at accuracy levels equivalent to models generated from ASO data collected on the day of interest. Lastly, although SWE distributions simulated in years with anomalous SWE distributions (2014, 2015) had the highest errors, models from these years still yielded good performance in 2013 and 2016. Thus, the benefit of ASO in anomalously dry years is two-fold: water managers receive accurate information during a year that is difficult to model, but also these observed SWE distributions can be used to simulate SWE distributions in future, less anomalous years. Overall, ASO provides an unprecedented observation of the relationships between SWE, fSCA,

and physiography. The ASO dataset facilitates improved understanding of these relationships in both time and space and should lead to better information for water managers.

8 Data Availability

All data and code is available at <https://osf.io/5643w/>

9 Acknowledgements

D. Schneider thanks his PhD committee for their insightful comments. The authors would like to acknowledge NASA for supporting D. Schneider with an Earth and Space Science Fellowship (NNX14AL27H) and funding the time of N.P. Molotch with grant numbers NNX17AF50G and 80NSSC17K0071.

10 References

- Anderson, E.: Snow Accumulation and Ablation Model, US Department of Commerce, Silver Spring, MD. 1973.
- Bair, E. H., Rittger, K. E., Davis, R. E., Painter, T. H. and Dozier, J.: Validating reconstruction of snow water equivalent in California's Sierra Nevada using measurements from the NASA Airborne Snow Observatory, *Water Resour. Res.*, n/a–n/a, doi:10.1002/2016WR018704, 2016.
- Balk, B. and Elder, E.: Combining binary decision tree and geostatistical methods to estimate snow distribution in a mountain watershed, *Water Resources Research*, 36(1), 13–26, doi:10.1029/1999WR900251, 2000.
- Barrett, A. P.: National Operational Hydrologic Remote Sensing Center SNOW Data Assimilation System (SNODAS) Products at NSIDC, National Snow and Ice Data Center, Boulder, CO, USA. 2003.
- Bloschl, G., Kirnbauer, R. and Gutknecht, D.: Distributed Snowmelt Simulations in an Alpine Catchment 1. Model Evaluation on the Basis of Snow Cover Patterns, *Water Resources Research*, 27(12), 3171–3179, doi:10.1029/91WR02250, 1991.
- Bühler, Y., Marty, M., Egli, L., Veitinger, J., Jonas, T., Thee, P. and Ginzler, C.: Snow depth mapping in high-alpine catchments using digital photogrammetry, *The Cryosphere*, 9(1), 229–243, doi:10.5194/tc-9-229-2015, 2015.
- Carroll, S. S. and Cressie, N.: A comparison of geostatistical methodologies used to estimate snow water equivalent - Reply, *Journal of the American Water Resources Association*, 33(1), 221–222, 1997.
- Clark, M. P., Hendrikx, J., Slater, A. G., Kavetski, D., Anderson, B., Cullen, N. J., Kerr, T., Örn Hreinsson, E. and Woods, R. A.: Representing spatial variability of snow water equivalent in hydrologic and land-surface models: A review, *Water Resources Research*, 47(7), doi:10.1029/2011WR010745, 2011.
- Cline, D. W., Bales, R. C. and Dozier, J.: Estimating the spatial distribution of snow in mountain basins using remote sensing and energy balance modeling, *Water Resources Research*, 34(5), 1275–1285, doi:10.1029/97WR03755, 1998.
- Clow, D. W., Nanus, L., Verdin, K. L. and Schmidt, J.: Evaluation of SNODAS snow depth and snow water equivalent estimates for the Colorado Rocky Mountains, USA, edited by M. Pelto and K. R. Richard, *Hydrological Processes*, 26(17), 2583–2591, doi:10.1002/hyp.9385, 2012.

609 Conrad, O., Bechtel, B., Bock, M., Dietrich, H., Fischer, E., Gerlitz, L., Wehberg, J., Wichmann, V. and Boehner, J.:
610 System for Automated Geoscientific Analyses (SAGA) v. 2.1.4, Geoscientific Model Development, 8(7), 1991–
611 2007, doi:10.5194/gmd-8-1991-2015, 2015.

612 Cressie, N. A. C.: Statistics for spatial data, J. Wiley. 1993.

613 Cristea, N. C., Breckheimer, I., Raleigh, M. S., HilleRisLambers, J. and Lundquist, J. D.: An evaluation of terrain-
614 based downscaling of fractional snow covered area data sets based on LiDAR-derived snow data and orthoimagery,
615 Water Resour. Res., 53(8), 6802–6820, doi:10.1002/2017WR020799, 2017.

616 Dadic, R., Mott, R., Lehning, M. and Burlando, P.: Wind influence on snow depth distribution and accumulation
617 over glaciers, J. Geophys. Res., 115(F1), n/a–n/a, doi:10.1029/2009JF001261, 2010.

618 Deems, J. S., Fassnacht, S. R. and Elder, K. J.: Interannual Consistency in Fractal Snow Depth Patterns at Two
619 Colorado Mountain Sites, J. Hydrometeor, 9(5), 977–988, doi:10.1175/2008JHM901.1, 2008.

620 Deems, J. S., Painter, T. H. and Finnegan, D. C.: Lidar measurement of snow depth: a review, Journal of Glaciology,
621 59(215), 467–479, doi:10.3189/2013JoG12J154, 2013.

622 Donald, J. R., Soulis, E. D., Kouwen, N. and Pietroniro, A.: A Land Cover-Based Snow Cover Representation for
623 Distributed Hydrologic-Models, Water Resour. Res., 31(4), 995–1009, doi:10.1029/94WR02973, 1995.

624 Dozier, J.: Mountain hydrology, snow color, and the fourth paradigm, Eos Trans. AGU, 92(43), 373–374,
625 doi:10.1029/2011EO430001, 2011.

626 Dozier, J., Painter, T. H., Rittger, K. E. and Frew, J. E.: Time–space continuity of daily maps of fractional snow
627 cover and albedo from MODIS, Advances in Water Resources, 31(11), 1515–1526,
628 doi:10.1016/j.advwatres.2008.08.011, 2008.

629 Dozier, J., Schneider, S. R. and McGinnis, D. F.: Effect of grain size and snowpack water equivalence on visible and
630 near-infrared satellite observations of snow, Water Resources Research, 17(4), 1213–1221,
631 doi:10.1029/WR017i004p01213, 1981.

632 Egli, L. and Jonas, T.: Hysteretic dynamics of seasonal snow depth distribution in the Swiss Alps, Geophys. Res.
633 Lett., 36(2), n/a–n/a, doi:10.1029/2008GL035545, 2009.

634 Elder, K., Dozier, J. and Michaelsen, J.: Snow accumulation and distribution in an Alpine Watershed, Water
635 Resources Research, 27(7), 1541–1552, doi:10.1029/91WR00506, 1991.

636 Elder, K., Rosenthal, W. and Davis, R. E.: Estimating the spatial distribution of snow water equivalence in a
637 montane watershed, Hydrological Processes, 12(10-11), 1793–1808, doi:10.1002/(SICI)1099-
638 1085(199808/09)12:10/11<1793::AID-HYP695>3.3.CO;2-B, 1998.

639 Erickson, T. A., Williams, M. W. and Winstal, A.: Persistence of topographic controls on the spatial distribution of
640 snow in rugged mountain terrain, Colorado, United States, Water Resour. Res., 41(4), W04014,
641 doi:10.1029/2003WR002973, 2005.

642 Erxleben, J., Elder, E. and Davis, R.: Comparison of spatial interpolation methods for estimating snow distribution
643 in the Colorado Rocky Mountains, Hydrological Processes, 16(18), 3627–3649, doi:10.1002/hyp.1239, 2002.

644 Fassnacht, S. R., Dressler, K. A. and Bales, R. C.: Snow water equivalent interpolation for the Colorado River Basin
645 from snow telemetry (SNOTEL) data, Water Resour. Res., 39(8), 1208, doi:10.1029/2002WR001512, 2003.

646 Fassnacht, S. R., Sexstone, G. A., Kashipazha, A. H., Jasinski, M. F., Kampf, S. K., Thaden, Von, B. C. and López
647 Moreno, J. I.: Deriving snow-cover depletion curves for different spatial scales from remote sensing and snow
648 telemetry data, *Hydrological Processes*, 30(11), 1708–1717, doi:10.1002/hyp.10730, 2016.

649 Friedman, J., Hastie, T. and Tibshirani, R.: Regularization Paths for Generalized Linear Models via Coordinate
650 Descent, *Journal of Statistical Software*, 33(1), 1–22, 2010.

651 Garvert, M. F., Smull, B. and Mass, C.: Multiscale Mountain Waves Influencing a Major Orographic Precipitation
652 Event, <http://dx.doi.org/10.1175/JAS3876.1>, 64(3), 711–737, doi:10.1175/JAS3876.1, 2007.

653 GDAL Development Team: GDAL - Geospatial Data Abstraction Library, Version 1.11.3. 2015.

654 Giersch, J. J., Hotaling, S., Kovach, R. P., Jones, L. A. and Muhlfeld, C. C.: Climate-induced glacier and snow loss
655 imperils alpine stream insects, *Glob Chang Biol*, 23(7), 2577–2589, doi:10.1111/gcb.13565, 2016.

656 Good, W. and Martinec, J.: Pattern recognition of air photographs for estimation of snow reserves, *Annals of*
657 *Glaciology*, 1987.

658 Grohmann, C. H., Smith, M. J. and Riccomini, C.: Multiscale Analysis of Topographic Surface Roughness in the
659 Midland Valley, Scotland, *Geoscience and Remote Sensing, IEEE Transactions on*, 49(1), 1200–1213,
660 doi:10.1109/TGRS.2010.2053546, 2011.

661 Grünewald, T., Stötter, J., Pomeroy, J. W., Dadic, R., Moreno Baños, I., Marturià, J., Spross, M., Hopkinson, C.,
662 Burlando, P. and Lehning, M.: Statistical modelling of the snow depth distribution in open alpine terrain, *Hydrol.*
663 *Earth Syst. Sci.*, 17(8), 3005–3021, doi:10.5194/hess-17-3005-2013, 2013.

664 Gutmann, E. D., Larson, K. M., Williams, M. W., Nievinski, F. G. and Zavorotny, V.: Snow measurement by GPS
665 interferometric reflectometry: an evaluation at Niwot Ridge, Colorado, *Hydrological Processes*, 26(19), 2951–2961,
666 2012.

667 Hall, D. K., Foster, J. L., Salomonson, V. V., Klein, A. G. and Chien, J. Y. L.: Development of a technique to assess
668 snow-cover mapping errors from space, *Geoscience and Remote Sensing, IEEE Transactions on*, 39(2), 432–438,
669 doi:10.1109/36.905251, 2001.

670 Harpold, A., Dettinger, M. and Rajagopal, S.: Defining snow drought and why it matters, *EOS - Earth & Space*
671 *Science News*, 98, doi:10.1029/2017EO068775, 2017.

672 Harshburger, B. J., Humes, K. S., Walden, V. P., Blandford, T. R., Moore, B. C. and Dezzani, R. J.: Spatial
673 interpolation of snow water equivalency using surface observations and remotely sensed images of snow-covered
674 area, *Hydrological Processes*, 24(10), 1285–1295, doi:10.1002/hyp.7590, 2010.

675 Hastie, T., Tibshirani, R. and Friedman, J.: *The Elements of Statistical Learning*, Springer New York, New York,
676 NY. 2009.

677 Jonas, T., Marty, C. and Magnusson, J.: *Journal of Hydrology*, *Journal of Hydrology*, 378(1-2), 161–167,
678 doi:10.1016/j.jhydrol.2009.09.021, 2009.

679 Kirnbauer, R. and Blöschl, G.: Wie ähnlich sind Ausaperungsmuster von Jahr zu Jahr (How similar are snow cover
680 patterns from year to year)? *Deutsche Wässerkundliche Mitteilungen*, 37(5/6), 113–121, 1994.

681 Koch, F., Prasch, M., Schmid, L., Schweizer, J. and Mauser, W.: Measuring Snow Liquid Water Content with Low-
682 Cost GPS Receivers, *Sensors* 2014, Vol. 14, Pages 20975–20999, 14(11), 20975–20999, doi:10.3390/s141120975,
683 2014.

684 König, M. and Sturm, M.: Mapping snow distribution in the Alaskan Arctic using aerial photography and
685 topographic relationships, *Water Resources Research*, 34(12), 3471–3483, doi:10.1029/98WR02514, 1998.

686 Lawrence, D. M., Oleson, K. W., Flanner, M. G., Thornton, P. E., Swenson, S. C., Lawrence, P. J., Zeng, X., Yang,
687 Z.-L., Levis, S., Sakaguchi, K., Bonan, G. B. and Slater, A. G.: Parameterization improvements and functional and
688 structural advances in Version 4 of the Community Land Model, *J. Adv. Model. Earth Syst.*, 3(3), M03001–n/a,
689 doi:10.1029/2011MS000045, 2011.

690 Lehning, M., Löwe, H., Ryser, M. and Raderschall, N.: Inhomogeneous precipitation distribution and snow transport
691 in steep terrain, *Water Resour. Res.*, 44(7), 123, doi:10.1029/2007WR006545, 2008.

692 Li, H., He, Y., Hao, X., Che, T., Wang, J. and Huang, X.: Downscaling Snow Cover Fraction Data in Mountainous
693 Regions Based on Simulated Inhomogeneous Snow Ablation, *Remote Sensing*, 7(7), 8995–9019,
694 doi:10.3390/rs70708995, 2015.

695 Liston, G. E.: Interrelationships among Snow Distribution, Snowmelt, and Snow Cover Depletion: Implications for
696 Atmospheric, Hydrologic, and Ecologic Modeling, *Journal of Applied Meteorology*, 38(10), 1474–1487,
697 doi:10.1175/1520-0450(1999)038<1474:IASDSA>2.0.CO;2, 1999.

698 Litaor, M. I., Williams, M. and Seastedt, T. R.: Topographic controls on snow distribution, soil moisture, and
699 species diversity of herbaceous alpine vegetation, Niwot Ridge, Colorado, *J. Geophys. Res.*, 113(G2), n/a–n/a,
700 doi:10.1029/2007JG000419, 2008.

701 Livneh, B., Xia, Y., Mitchell, K. E., Ek, M. B. and Lettenmaier, D. P.: Noah LSM Snow Model Diagnostics and
702 Enhancements, *J. Hydrometeorol.*, 11(3), 721–738, doi:10.1175/2009JHM1174.1, 2010.

703 López-Moreno, J. I. and Nogués-Bravo, D.: Interpolating local snow depth data: an evaluation of methods,
704 *Hydrological Processes*, 20(10), 2217–2232, doi:10.1002/hyp.6199, 2006.

705 López-Moreno, J. I., Fasnacht, S. R., Heath, J. T., Musselman, K. N., Revuelto, J., Latron, J. B. P., Morán-Tejeda,
706 E. and Jonas, T.: Small scale spatial variability of snow density and depth over complex alpine terrain: Implications
707 for estimating snow water equivalent, *Advances in Water Resources*, 55, 40–52,
708 doi:10.1016/j.advwatres.2012.08.010, 2013.

709 López-Moreno, J. I., Revuelto, J., Fasnacht, S. R., Azorín-Molina, C., Vicente-Serrano, S. M., Morán-Tejeda, E.
710 and Sextone, G. A.: Snowpack variability across various spatio-temporal resolutions, *Hydrological Processes*,
711 29(6), 1213–1224, doi:10.1002/hyp.10245, 2014.

712 Luce, C. H. and Tarboton, D. G.: The application of depletion curves for parameterization of subgrid variability of
713 snow, *Hydrological Processes*, 18(8), 1409–1422, doi:10.1002/hyp.1420, 2004.

714 Luce, C. H., Tarboton, D. G. and Cooley, K. R.: Sub-grid parameterization of snow distribution for an energy and
715 mass balance snow cover model, *Hydrological Processes*, 13(12-13), 1921–1933, doi:10.1002/(SICI)1099-
716 1085(199909)13:12/13<1921::AID-HYP867>3.0.CO;2-S, 1999.

717 Marchand, W. D. and Killingtveit, A.: Statistical probability distribution of snow depth at the model sub-grid cell
718 spatial scale, *Hydrological Processes*, 19(2), 355–369, doi:10.1002/hyp.5543, 2005.

719 Marks, D., Domingo, J., Susong, D., Link, T. and Garen, D.: A spatially distributed energy balance snowmelt model
720 for application in mountain basins, *Hydrological Processes*, 13(12-13), 1935–1959, doi:10.1002/(SICI)1099-
721 1085(199909)13:12/13<1935::AID-HYP868>3.0.CO;2-C, 1999.

722 Marshall, H.-P. and Koh, G.: FMCW radars for snow research, *Cold Regions Science and Technology*, 52(2), 118–
723 131, 2008.

724 Martinec, J. and Rango, A.: Areal distribution of snow water equivalent evaluated by snow cover monitoring, *Water*
725 *Resour. Res.*, 17(5), 1480–1488, 1981.

726 Meromy, L., Molotch, N. P., Link, T. E., Fassnacht, S. R. and Rice, R.: Subgrid variability of snow water equivalent
727 at operational snow stations in the western United States, *Hydrological Processes*, 27(17), 2383–2400,
728 doi:10.1002/hyp.9355, 2012.

729 Mizukami, N. and Perica, S.: Spatiotemporal Characteristics of Snowpack Density in the Mountainous Regions of
730 the Western United States, *Journal of Hydrometeorology*, 9(6), 1416–1426, doi:10.1175/2008JHM981.1, 2008.

731 Molotch, N. P. and Bales, R. C.: Scaling snow observations from the point to the grid element: Implications for
732 observation network design, *Water Resources Research*, 41(11), doi:10.1029/2005WR004229, 2005.

733 Molotch, N. P. and Bales, R. C.: SNOTEL representativeness in the Rio Grande headwaters on the basis of
734 physiographics and remotely sensed snow cover persistence, *Hydrological Processes*, 20(4), 723–739,
735 doi:10.1002/hyp.6128, 2006.

736 Molotch, N. P. and Margulis, S. A.: Estimating the distribution of snow water equivalent using remotely sensed
737 snow cover data and a spatially distributed snowmelt model: A multi-resolution, multi-sensor comparison, *Advances*
738 *in Water Resources*, 31(11), 1503–1514, doi:10.1016/j.advwatres.2008.07.017, 2008.

739 Molotch, N. P., Colee, M. T., Bales, R. C. and Dozier, J.: Estimating the spatial distribution of snow water
740 equivalent in an alpine basin using binary regression tree models: the impact of digital elevation data and
741 independent variable selection, *Hydrological Processes*, 19(7), 1459–1479, doi:10.1002/hyp.5586, 2005.

742 Niu, G.-Y. and Yang, Z.-L.: An observation-based formulation of snow cover fraction and its evaluation over large
743 North American river basins, *J. Geophys. Res.*, 112(D21), doi:10.1029/2007JD008674, 2007.

744 Niu, G.-Y., Yang, Z.-L., Mitchell, K. E., Chen, F., Ek, M. B., Barlage, M., Kumar, A., Manning, K., Niyogi, D.,
745 Rosero, E., Tewari, M. and Xia, Y.: The community Noah land surface model with multiparameterization options
746 (Noah-MP): 1. Model description and evaluation with local-scale measurements, *J. Geophys. Res.*, 116(D12), n/a–
747 n/a, doi:10.1029/2010JD015139, 2011.

748 Nolan, M., Larsen, C. F. and Sturm, M.: Mapping snow-depth from manned-aircraft on landscape scales at
749 centimeter resolution using Structure-from-Motion photogrammetry, *The Cryosphere Discuss.*, 9(1), 333–381,
750 doi:10.5194/tcd-9-333-2015, 2015.

751 NPS: Plants - Yosemite National Park, [online] Available from: <https://www.nps.gov/yose/learn/nature/plants.htm>
752 (Accessed 5 October 2016), 2016.

753 Painter, T. H., Berisford, D. F., Boardman, J. W., Bormann, K. J., Deems, J. S., Gehrke, F., Hedrick, A., Joyce, M.,
754 Laidlaw, R., Marks, D., Mattmann, C., McGurk, B., Ramirez, P., Richardson, M., Skiles, S. M., Seidel, F. C. and
755 Winstral, A.: The Airborne Snow Observatory: Fusion of scanning lidar, imaging spectrometer, and physically-
756 based modeling for mapping snow water equivalent and snow albedo, *Remote Sensing of Environment*, 184, 139–
757 152, doi:10.1016/j.rse.2016.06.018, 2016.

758 Painter, T. H., Rittger, K. E., McKenzie, C., Slaughter, P., Davis, R. E. and Dozier, J.: Retrieval of subpixel snow
759 covered area, grain size, and albedo from MODIS, *Remote Sensing of Environment*, 113(4), 868–879,
760 doi:10.1016/j.rse.2009.01.001, 2009.

761 Parajka, J. and Bloeschl, G.: Spatio-temporal combination of MODIS images - potential for snow cover mapping,
762 *Water Resources Research*, 44(3), doi:10.1029/2007WR006204, 2008.

763 Parsons, W. J. and Castle, G. H.: Aerial reconnaissance of mountain snow fields for maintaining up-to-date forecasts
764 of snow melt runoff during the melt season, *Western Snow Conference*, Reno, Nevada. 1959.

765 Potts, H. L.: Snow surveys and runoff forecasting from photographs, Proceedings of the 5th Annual Western
766 Interstate Snow Survey Conference, 1937.

767 Potts, H. L.: A photographic snow survey method of forecasting runoff, Proceedings of the 12th Annual Western
768 Interstate Snow Survey Conference, 1944.

769 Prokop, A.: Assessing the applicability of terrestrial laser scanning for spatial snow depth measurements, Cold
770 Regions Science and Technology, 54(3), 155–163, doi:10.1016/j.coldregions.2008.07.002, 2008.

771 Raleigh, M. S., Rittger, K. E., Moore, C. E., Henn, B., Lutz, J. A. and Lundquist, J. D.: Ground-based testing of
772 MODIS fractional snow cover in subalpine meadows and forests of the Sierra Nevada, Mon. Wea. Rev., 128, 44–57,
773 doi:10.1016/j.rse.2012.09.016, 2013.

774 Revuelto, J., Jonas, T. and López Moreno, J. I.: Backward snow depth reconstruction at high spatial resolution based
775 on time-lapse photography, Hydrological Processes, 30(17), 2976–2990, doi:10.1002/hyp.10823, 2016.

776 Revuelto, J., López-Moreno, J. I., Azorín-Molina, C. and Vicente-Serrano, S. M.: Topographic control of snowpack
777 distribution in a small catchment in the central Spanish Pyrenees: intra- and inter-annual persistence, The
778 Cryosphere, 8(5), 1989–2006, doi:10.5194/tc-8-1989-2014, 2014.

779 Rice, R. and Bales, R. C.: Embedded-sensor network design for snow cover measurements around snow pillow and
780 snow course sites in the Sierra Nevada of California, Water Resources Research, 46(3), W03537, 2010.

781 Rice, R., Bales, R. C., Painter, T. H. and Dozier, J.: Snow water equivalent along elevation gradients in the Merced
782 and Tuolumne River basins of the Sierra Nevada, Water Resour. Res., 47, doi:10.1029/2010WR009278, 2011.

783 Rittger, K. E., Painter, T. H. and Dozier, J.: Assessment of methods for mapping snow cover from MODIS,
784 Advances in Water Resources, 51, 367–380, doi:10.1016/j.advwatres.2012.03.002, 2013.

785 Rosenthal, W. and Dozier, J.: Automated Mapping of Montane Snow Cover at Subpixel Resolution from the
786 Landsat Thematic Mapper, Water Resources Research, 32(1), 115–130, doi:10.1029/95WR02718, 1996.

787 Rutter, N., Cline, D. and Li, L.: Evaluation of the NOHRSC snow model (NSM) in a one-dimensional mode, Journal
788 of Hydrometeorology, 9(4), 695–711, doi:10.1175/2008JHM861.1, 2008.

789 Salomonson, V. V. and Appel, I.: Estimating fractional snow cover from MODIS using the normalized difference
790 snow index, Remote Sensing of Environment, 89(3), 351–360, doi:10.1016/j.rse.2003.10.016, 2004.

791 Sappington, J. M., Longshore, K. M. and Thompson, D. B.: Quantifying Landscape Ruggedness for Animal Habitat
792 Analysis: A Case Study Using Bighorn Sheep in the Mojave Desert, Journal of Wildlife Management, 71(5), 1419–
793 1426, doi:10.2193/2005-723, 2007.

794 Schirmer, M., Wirz, V., Clifton, A. and Lehning, M.: Persistence in intra-annual snow depth distribution:
795 I. Measurements and topographic control, Water Resources Research, 47(9), W09516–n/a,
796 doi:10.1029/2010WR009426, 2011.

797 Schneider, D. and Molotch, N. P.: Real-Time Estimation of Snow Water Equivalent in the Upper Colorado River
798 Basin using MODIS-based SWE Reconstructions and SNOTEL data, Water Resources Research,
799 doi:10.1002/2016WR019067, 2016.

800 Slater, A. G., Barrett, A. P., Clark, M. P., Lundquist, J. D. and Raleigh, M. S.: Uncertainty in seasonal snow
801 reconstruction: Relative impacts of model forcing and image availability, Advances in Water Resources, 55(0), 165–
802 177, doi:10.1016/j.advwatres.2012.07.006, 2013.

803 Stewart, I. T., Cayan, D. R. and Dettinger, M. D.: Changes toward earlier streamflow timing across western North
804 America, *Journal of Climate*, 18(8), 1136–1155, 2004.

805 Sturm, M. and Wagner, A. M.: Using repeated patterns in snow distribution modeling: An Arctic example, *Water*
806 *Resour. Res.*, 46(12), n/a–n/a, doi:10.1029/2010WR009434, 2010.

807 Sturm, M., Taras, B., Liston, G. E., Derksen, C., Jonas, T. and Lea, J.: Estimating Snow Water Equivalent Using
808 Snow Depth Data and Climate Classes, *Journal of Hydrometeorology*, 11(6), 1380–1394,
809 doi:10.1175/2010JHM1202.1, 2010.

810 Trujillo, E., Ramirez, J. A. and Elder, K. J.: Scaling properties and spatial organization of snow depth fields in sub-
811 alpine forest and alpine tundra, *Hydrological Processes*, 23(11), 1575–1590, doi:10.1002/hyp.7270, 2009.

812 Veitinger, J., Sovilla, B. and Purves, R. S.: Influence of snow depth distribution on surface roughness in alpine
813 terrain: a multi-scale approach, *The Cryosphere*, 8(2), 547–569, doi:10.5194/tc-8-547-2014, 2014.

814 Walters, R. D., Watson, K. A., Marshall, H.-P., McNamara, J. P. and Flores, A. N.: A physiographic approach to
815 downscaling fractional snow cover data in mountainous regions, *Remote Sensing of Environment*, 152, 413–425,
816 doi:10.1016/j.rse.2014.07.001, 2014.

817 Xia, Q., Gao, X., Chu, W. and Sorooshian, S.: Estimation of daily cloud-free, snow-covered areas from MODIS
818 based on variational interpolation, *Water Resour. Res.*, 48(9), 1480–1488, doi:10.1029/WR017i005p01480, 2012.

819 Zou, H. and Hastie, T.: Regularization and variable selection via the elastic net, *Journal of the Royal Statistical*
820 *Society Series B-Statistical Methodology*, 67(2), 301–320, doi:10.1111/j.1467-9868.2005.00503.x, 2005.

821

822